Universidad Zaragoza

Master Thesis

Title of Thesis

3D Numerical Modeling of Cell Migration and Cell-Cell Interaction

Presented by

SEYED JAMALEDDIN MOUSAVI

Supervised by

MOHAMED HAMDY DOWEIDAR
Dr. Industrial Engineering

Presented at

University of Zaragoza
Department of Mechanical Engineering
September 2012

Acknowledgements

I would like to express my greatest gratitude to the persons who have helped and supported me throughout this work. I am grateful to my supervisor, Dr. Mohamed Hamdy Doweidar, for his continuous support during my study, from initial advice and contacts in the early stages of conceptual inception and his encouragement to this day.

Special thanks of mine goes to Professor Manule Doblaré who accepted me for PhD in GEMM group, without his support this dissertation could not have been done.

I would like to thank Dr. Pilar Martín Duque for her kind collaboration in experimental part of this dissertation in "Instituto Aragonés de Ciencias de la Salud (I+CS)".

I wish to appreciate Iñaki, Raquel, Clara, and Alan, without their kind support and contribution, the experimental part of this dissertation would not have implemented.

Many friends have helped me to have a great time through these two years. Their support and care helped me overcome setbacks and stay focused on my graduate study. I greatly value their friendship and I deeply appreciate their belief in me. I am also grateful to Olfa for her moral support, to Sara who helped me a lot specially with administrative works, and to Siamak who shared his experience with me.

Also great thanks to my family, specially my mother, who tried her best to support me by giving me a lot of encouragement during schooling.

Words fail me to express my sincere appreciation to my wife Solmaz whose love, dedication and persistent confidence in me, have taken the load off my shoulder. I owe for her great patience, that made this dissertation possible.

Abstract

Cell migration is one of the significant aspects to be taken into account in many physiological processes, such as wound healing, cancer development, morphogenesis, and the immune response. It is well known that in these processes and many others, cell migration is partially guided by mechanical properties of its substrate as well as specific chemoattractants. Although many experimental works have been developed to understand the effect of the mechanical properties of the substrate onto cell migration, accurate 3D cell locomotion models have not presented yet. In this work I present a 3D model for migration of a single cell as well as population of cells. In the presented model I assume that the cell follows two main processes, firstly sensing its interface with the substrate to determine the migration direction, secondly exerting subsequent forces to move. The cell traction forces are considered to depend on the internal cell deformation during the sensing step. A random protrusion force is also considered that affect on the cell migration and speed. This model was applied for one single cell getting results in agreement with available experimental and numerical data. The model has been also applied to a substrate with stiffness gradient and to a substrate with changing depth. The results corroborate previous experimental results in the sense that the cell tendency is always to migrate from softer to stiffer regions. In very special cases, however, cells may change their tendency and migrate towards softer parts of the substrate till an imaginary equilibrium plane whose location depends on the mechanical properties of the substrate. Furthermore, cells tend to migrate toward fixed boundaries. In case of surface migration, cell tends to migrate toward less thicker substrates. In case of interaction between two cells, the results demonstrate that their interaction decreases the mean migration speed while increase local migration speed. This process also takes place for high cell population as cells tend to aggregate in small slugs and then these slugs join together in middle of the substrate creating bigger aggregations.

Contents

List of Figures

List of Tables

Introduction

Cell migration is a broad term referring to processes which include movement of cells from one position to another. It may carry out during in vitro cell culture or within multicellular organisms (in vivo precess). The importance of cell migration is due to its notable role in physiological, biological and pathological processes such as tissue morphogenesis [22], cell differentiation [36], cell proliferation [3], cancer development [25, 37, 46, 50], wound healing [27], as well as in tissue engineering applications [14]. Such as cruise control device for setting car speed or a thermostat that controls air conditioners and heating devices, the obtained information in sensing scheme by the cell can control a range of processes, including cell migration and spreading, as well as cell differentiation. The cell behavior during locomotion in or on a substrate is not completely clear for scientists yet. However, it has been conclusively demonstrated that biochemical, biophysical and mechanical factors strongly affect on cell migration [9, 10, 17, 26, 30, 32, 35]. In particular, mechanical changes in cell substrate, such as those on bound adhesive ligands, topographical features, and stiffness distribution are all thought to guide and control cell migration [17].
The physical process of cell migration involves a number of coordinated events. There are two main processes involved in cell migration [44]: the first is sensing of its environment, the second is the generation of contractile forces by the actin-myosin apparatus in cell cytoskeleton driving forward the translocation of the cell body and causing traction forces on its substrate [23]. These steps involve the continuous rearrangement of cytoskeletal elements and cell-extracellular matrix (ECM) interactions. Briefly, these steps are distinguished by the formation of new adhesions, the development of traction, and abandoning old adhesions [23, 43]. Increasing intracellular forces or substrate stiffness induce more stable cell-matrix adhesions that are promoted to strengthen and grow, being this effect responsible of the cell tendency to move towards stiffer substrates [11].

State of the art

The mechanisms behind cell migration are not completely understood. However, there are many mathematical models which qualify the cell motility in 2D substrates [28, 49, 51]. But there exit only few 3D mathematical models describing cell behavior [5, 6, 52]. Generally, there are two types of model reported in literature. The first is based on a continuum approach which supposes the cell as a continuum structure with special mechanical properties. . While the second is a micro/nanostructural approach describing the cytoskeleton (CSK) as a principal structural unit which is developed to investigate cytoskeletal mechanics in adherent cells [2]. The former model is easier and simpler to compute the large deformations of the cell. Besides, continuum models may be useful to understand the distribution of stresses and strains, trans-

mitting of resultant forces to the CSK.
Experimental works by Lo and et al. [26] demonstrated that cell is able to determine substrate rigidity by monitoring the magnitude of counterforces upon the consumption of a given amount of energy, i.e., strong mechanical feedback from the stiff substrate occurs after a small reception of displacement. Since elastic energy is the integration of forces along the distance, with the same amount of energy consumption, soft substrates can generate a weaker mechanical feedback but a longer displacement [26]. On the other hand, the stronger mechanical feedback in stiffer substrates may lead to the activation of stress-sensitive ion channels [24]. These responses may, in turn, regulate the extent of protein tyrosine phosphorylation, the stability of focal adhesions, and the strength of contractile forces [34].
Migration of high population of cells inside a substrate is one of the main aspects of tissue formation [12]. There are several previous methods to model high population of cells in a multicellular system, a good survey can be found in [32]. One of main problems with some previous models is that they ignore to properly balance the active movement forces generated by each individual cell affecting cell-cell interaction [41]. Also some of them don't consider effective forces like traction, drag and protrusion forces that acting on cell during migration [29]. Besides, most of them are two dimensional models [7, 8, 15].

Description of the thesis

The present work can be considered as an extension of the previous model presented by Borau et al. [5, 6]. They developed a model to simulate single cell migration in 3D substrates but with several limitations which are improved herein. It can be said that their model is applicable only for a single cell. Besides, they considered cell as a hexahedral element, therefore, cell has a cubic form which is far from reality and may cause inaccurate results. Moreover, reorientation of cell is based on the projective alignment with the resultant of the principal stress directions. Reorientation according to maximum principle stresses was not too accurate in that paper, since the stresses in the element integration point were projected onto the nodes, being therefore an average of the projected strains and stresses. Here for determination of the cell migration I use a criterion based on displacements of external nodes of the cell with respect to its centroid (internal cell deformation). In the presented model, not only there is no limitation for the number of embedded cells and the number of elements which represent the cell, but also cell can have any shape configuration. However, the presented simulations have been carried out for a semi-sphere cell shape configuration in case of surface locomotion while for a 3D migration a spherical cell shape configuration is considered.
In this work, I investigate the effects of substrate mechanical properties on cell migration as well as cell-cell interactions. A 3D finite element model to simulate cell migration within 3D substrates is developed and extended to consider cell-cell interaction. Several numerical experiments are presented to demonstrate the predictive capability of the presented model for both cases of single cell and of cell population. To verify our model, beside to the existed experimental data, the numerical experiments presented by Borau et al. [5, 6] were reproduced, the obtained results were totally consistent with their results. Then, the presented model was applied to a substrate with stiffness gradient and free boundary surfaces [17]. The results illustrate that the cell tendency is to migrate in direction of the stiffness gradient in a random path until achieving an imaginary equilibrium plane (IEP) located far from the free boundary

surfaces. Once the cell arrives to this IEP, it randomly moves around that plane.
Our model is also applicable for surface cell migration. I used it to study the effect of substrate depth on cell locomotion. The results demonstrate that the cell tends to migrate toward minimum depth [9, 10].
Since the phenomenon of cell-cell interaction is not considered in previous numerical models, I extended our model to represent the locomotion of cell population. In case of only two cells, simulations show that there is a tendency between them to migrate toward each other. This phenomenon, in general, decreases their overall migration velocity. Once they are in contact, they stay together until the protrusion force changes their polarization direction and they may separate. This process is frequently repeated while cells migrate toward stiffer regions of the substrate. In the last experiment, 40 cells are simultaneously embedded within a constant stiffness substrate. As they start to move, their interaction causes that they aggregate in slugs in the middle of the substrate. This process can be considered as a step forward toward tissue generation.

Chapter 1

Finite Element Model

Cells have a special internal structure which is able to sense the stiffness of the matrix in which they reside. For instance, fibroblasts preferentially move toward stiffer substrates [20, 28]. This phenomenon is known as mechanotaxis in which a cell moves directionally following a mechano-sensing process [35]. In the mechano-sensing step, the cell senses its substrate by exerting a sensing force to diagnose its surroundings, and consequently, gets some information about its substrate rigidity. Once the cell has determined its surrounding mechanical conditions, it starts to pull itself towards the stiffer and/or more fixed region.
The cellular elements with a relevant function in the cell mechano-sensing mechanics are the actin bundles, the actomyosin contractile apparatus and the passive mechanical strength of the rest of the cell body, whose main contribution is related to the action of the cytoskeleton microtubules and the membrane (Fig. 1.1) [9, 28, 32, 34, 35]. The cytoplasmic CSK is linked with the external ECM through focal adhesions and trans-membrane integrins that are assumed totally rigid for the present model. This scheme agrees with the tensegrity hypothesis [20], since deformation of external substrate is balanced by tensile forces generated in the actin CSK. External forces are also considered to be another possible cause of the deformation of the substrate and cell. The presented model can be used to simulate adherent cells cultured on 2D substrates, cultured in 3D hydro-gels, on the surface of a scaffold or attached to the ECM of a connective tissue, regardless of their real environment. ECM and substrate will be used therefore without distinction in this work.
In this chapter I will present a numerical model to describe effective stresses and forces on a single cell migration and then I will discuss how to extend it to cell population.

1.1 Model formulation

In the same line of Borau et al. [5, 6], the one-dimensional model represented in Fig. 1.2-a can be particularized to octahedral or hydrostatic stresses. Assuming that contractile forces exerted by cells are isotropic [28], the change of length of each element is then interpreted as its corresponding volumetric strain [48]. In such a case, the characteristic spring constant can be identified with the volumetric stiffness modulus of the representative element. The physical interpretation of the variables in each branch of the model is then: K_{pas}, K_{act} and K_{subs} denote the stiffnesses of microtubules, myosin II and substrate respectively, ϵ_1 represents the minimum volumetric strain, ϵ_2 is the maximum volumetric strain of the cell [28], σ_{act} stands for the mean contractile stress generated internally by the myosin II machinery and transmitted through the actin bundles; σ_{pas} denotes the contractile stress supported by the passive resistance of the cell,

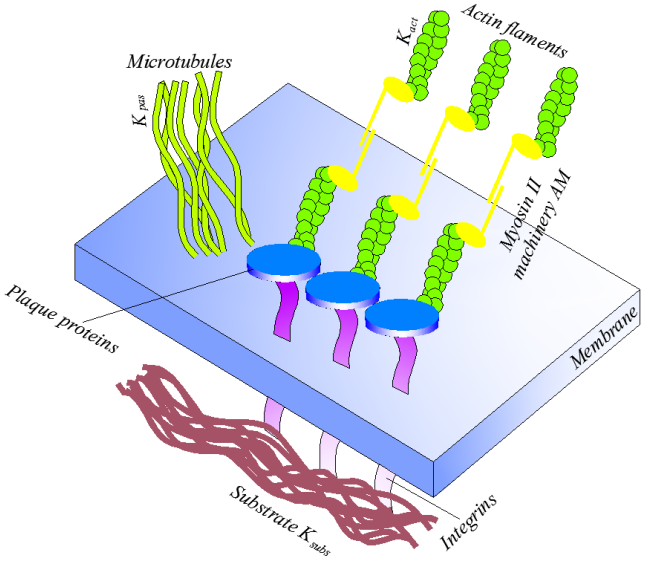

Figure 1.1: Schematic diagram of the relevant mechanical constituents of a cell [28].

essentially corresponding to the CSK microtubules and to the membrane; σ_s is the stress of the ECM, and f_{ext} denotes external forces. The effective stress transmitted by the cell to the ECM, σ_{cell}, is therefore given by

$$\sigma_{cell} = \sigma_{pas} + \sigma_{act} \tag{1.1}$$

It may be interpreted as this part of the active stress that is not absorbed by the microtubules. Forces from both microtubules, σ_{pas}, and actin bundles, σ_{act}, are exerted to the proteins plaque (Fig. 1.1) [28]. Thereby, σ_{cell} can also be interpreted as the average cell stress that bears the submembrane plaque in agreement with the integrin-mediated mechano-sensing hypothesis [4]. In addition, ϵ denotes local volumetric strain. In the model herein presented, local strain is computed from the deformation of the cell external nodes along the direction of the traction force exerted at the corresponding node. ϵ_{act} stands for deformation of the active contractile element. This deformation relates to the fact that the real physical change of the overlap between myosin and actin filaments occurs when active forces are applied. Eventually, ϵ_a represents the deformation of the actin bundles that promote the active forces transmitted.
We approximated the cell unidimensional constitutive behavior by a simple linear-elastic spring [28], which is a reasonable simplification of cell-substrate structure under moderate cell and substrate strains. Besides, interaction between the actin and myosin is considered as an active force arisen from a relative sloping between actin and myosin filaments. It is motivated by myosin cross-bridges on hydrolysis of adenosine triphosphate (ATP). The reaction by which chemical energy stored transmits into high energy of phosphoanhydric bonds in ATP [45] is maximal for an optimal filament overlap and decreases proportionally with decreasing overlapping [39]. Therefore, for calculation of the contractile stress, σ_{act}, as a function of deformation of the contractile elements, a simple piecewise linear constitutive model has been used. As seen in Fig. 1.2-b, if deformation of cell is in the ϵ_1-ϵ_2 range, the active stress has effect on net stress transmitted by the cell, else it will be zero. Thus in the ϵ_1-ϵ_2 range, it can be calculated as

$$\sigma_{act} = \frac{K_{act}\sigma_{max}(\epsilon_i - \epsilon)}{K_{act}\epsilon_i - \sigma_{max}} \tag{1.2}$$

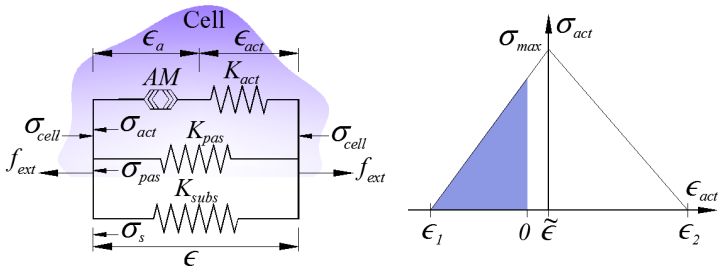

(a) (b)

Figure 1.2: Mechano-sensing model of an adherent cell. (a) Cell mechanical model. K_{act}, K_{pas}, and K_{subs}, denote the stiffness modulus of actin filaments, of the passive components of the cell and of the substrate, respectively. f_{ext} stands for external forces applied to the cell or the substrate. (b) Dependence of the contractile stress, σ_{act}, on the deformation of the contractile element, ϵ_{act}. σ_{max}, stands for the maximum contractile stress exerted by the actin-myosin machinery, ϵ_1 and ϵ_2 are the corresponding shortening and lengthening strains of the contractile elements with respect to the unloaded length at which active stress becomes zero [28].

where i=1 for $\epsilon_1 \leq \epsilon \leq \tilde{\epsilon}$ and i=2 for $\tilde{\epsilon} \leq \epsilon \leq \epsilon_2$, while $\tilde{\epsilon} = \sigma_{max}/K_{act}$. The passive resistance of the cell, σ_{pas}, is given by

$$\sigma_{pas} = K_{pas}\epsilon \tag{1.3}$$

Therefore by substitution of equations (1.2) and (1.3) in (1.1) the net stress transmitted to the ECM by a single cell as a function of the ECM volumetric strain, ϵ, can be calculated as

$$\sigma_{cell} = \begin{cases} K_{pas}\epsilon & \epsilon < \epsilon_1 \quad \text{or} \quad \epsilon > \epsilon_2 \\ K_{pas}\epsilon + \frac{K_{act}\sigma_{max}(\epsilon_1 - \epsilon)}{K_{act}\epsilon_1 - \sigma_{max}} & \epsilon_1 \leq \epsilon \leq \tilde{\epsilon} \\ K_{pas}\epsilon + \frac{K_{act}\sigma_{max}(\epsilon_2 - \epsilon)}{K_{act}\epsilon_2 - \sigma_{max}} & \tilde{\epsilon} \leq \epsilon \leq \epsilon_2 \end{cases} \tag{1.4}$$

In the physical process of cell locomotion, the contraction of the actin-myosin apparatus drives forward the translocation of the cell body and causes traction forces on the substrate [26, 44]. Actually, the movement of cells within a complex embryo or organism is guided by a complex interplay between chemical and physical signals like substrate stiffness [17, 26], boundary conditions and generated forces due to cell-cell and cell-substrate interactions [26, 44]. Anyway, the simplified model described above is here used to predict cell migration as a function of cell internal deformation.

The prominent aspect of the presented approach for cell modeling is that the cell can have any shape and can be represented by any number of finite elements. For this purpose, an algorithm has been used to track the key parameters required for migration at each time step considering important processes for cell migration, such as asymmetry of the cell, traction force, and traction force generation. Moreover, several aspects associated to the substrate such as stiffness, boundary conditions and their effects on the direction of cell locomotion have been taken into account.

To calculate the velocity and the new position of the cell within the substrate at each time step, the total net force during cell movement is balanced. In this case, the time step needed for model discretization is equal to the time of one cycle of cell migration that is the time taken by the cell to become sufficiently attached to its substrate in its advancing front and simultaneously break the adhesion with the substrate in the trailing back. It can change regarding to the

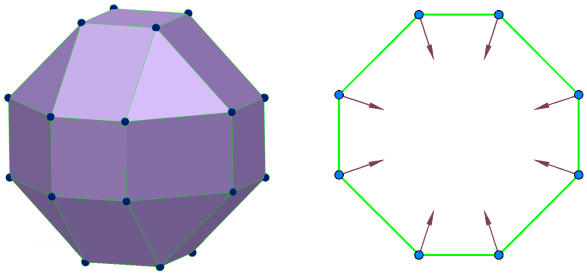

(a) (b)

Figure 1.3: (a) 3D spherical shape configuration of the cell. (b) Exerted sensing forces at every external node of the cell toward its centroid.

deformation of the cell, traction and protrusion forces and the cell speed at every step. Time of one complete cycle of cell migration for fibroblast, epithelial or endothelial cells is around 600 seconds [44].
The considered effective forces which act on cell and substrate are traction forces, drag forces, and protrusion forces [26, 35, 44]. The traction forces are the result of traction at the front and the rear of the cell and depend on the force per ligand-receptor complex due to their different adhesiveness. These two forces at the back and front of the cell can be mathematically represented as [52]

$$F_{trac} \mid_{f,b} = \sigma_{cell} S\zeta \mid_{f,b} \tag{1.5}$$

where σ_{cell}, cell stress, can be calculated from Eq. 1.4. S stands for a proportionality model parameter with units of area and ζ is the adhesiveness that takes into account different numbers of receptors at the front and the rear of cell and binding strength of these receptors to the ligand in the ECM [52] and is given by

$$\zeta = kn\psi \tag{1.6}$$

The value of ζ is different at the front and the rear of the cell because there are different number of receptors and the binding stress of each of those receptors may be also different. k is the binding constant for the integrins at the front and end of the cell to the ligands in the ECM (in mol^{-1}). For present simulations, I assume that the binding constant is equal for both front and rear of the cell. n is the total number of available receptors at the front or back of the cell and it is assumed that $n_f > n_b$ (in mol). This means that as cell polarizes, the distribution of integrins will be asymmetrically distributed on the cell surface [52]. Finally, ψ represents the concentration of the ligands at the leading edge of the cell in the ECM. Consequently, F_{trac} may be written as

$$F_{trac} = \sigma_{cell} S(kn\psi \mid_f - kn\psi \mid_b) \tag{1.7}$$

The second force which affects the cell is the resistive force (drag force) which comes from the viscous resistance to motility. In a Maxwell solid, the needed force for deforming the ECM depends on the deformation rate and accordingly the velocity. As the main objective here is to imply a velocity dependent opposing force associated to the viscoelastic character of the cell surrounding ECM, so, and for simplification, I assume the ECM as a viscoelastic medium [52].

In this case, the drag force can be defined as

$$F_{drag} = \beta \mu v \tag{1.8}$$

where μ is the effective viscosity of the viscoelastic matrix, it is considered as a constant throughout the substrate, v denotes the velocity of cell relative to the substrate. The constant β depends on the cell shape [52]. In the ideal case of a spherical cell moving through Newtonian infinitely viscose medium, β can be approximated as [52]

$$\beta = 6\pi r \tag{1.9}$$

where r is the radius of the cell.
It is necessary to note that if the cell migrates through a purely elastic substrate, the force required for deforming the matrix will not depend on the velocity. Therefore a more realistic representation of the opposing force would be the summation of two contributions, one depending on cell velocity and the other independent [18, 21]. This is why the protrusion force has been introduced to be independent from cell velocity. Therefore, an effective guidance system appears in which cells send out local protrusions to probe the mechanical properties of the environment [26]. This force is generated by actin polymerization and cell or substrate attachments at the new location of lamellipodia protrusion, distinct from the cytoskeletal contractile force transmitted to the ECM [52]. It is a random force whose order of magnitude is the same to that of the traction force and less than it at every time step [21, 38]. Therefore, force equilibrium should be satisfied during cell locomotion, hence

$$\mathbf{F}_{trac} + \mathbf{F}_{prot} + \mathbf{F}_{drag} = 0 \tag{1.10}$$

Through this presented work, neither degradation nor remodeling of the ECM during cell locomotion are considered.

1.1.1 Single cell orientation

At every step, the cell exerts a sensing force to diagnose its environment and hence it can determine the direction of migration within the substrate. I suppose that this sensing force is exerted at each external finite element node of the elements that represent the cell toward the cell centroid (Fig. 1.3-b). The deformed cell subjected to those sensing forces is represented by dotted lines in Fig. 1.4. So, the cell internal strain for each external node of the cell can be written as

$$\epsilon_{cell} = \frac{AB}{OA} \tag{1.11}$$

Once the displacements of all nodes are calculated, information needed to compute ϵ_{cell} is available. Using Eq. 1.4, σ_{cell} at every external node of the cell can be calculated. Therefore, at each external node of the cell, the traction force vector can be represented by

$$\mathbf{F}_i^{trac} = F_i^{trac} \mathbf{e}_i \tag{1.12}$$

where F_i^{trac} is the magnitude of the traction force corresponding to the ith external node of the cell obtained from Eq. 1.7. $\mathbf{e}_i$ is a unit vector standing along the ith external node and the cell centroid which can be obtained by

$$\mathbf{e}_i = \frac{\mathbf{x}_o - \mathbf{x}_i}{\| \mathbf{x}_o - \mathbf{x}_i \|} \tag{1.13}$$

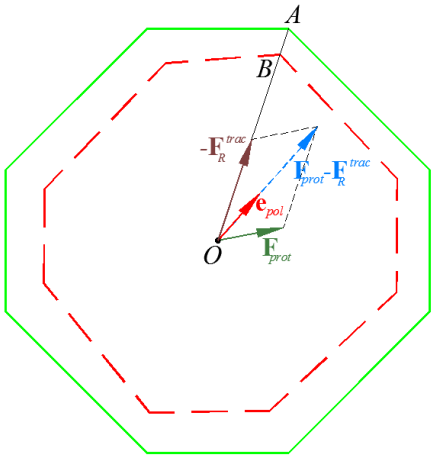

Figure 1.4: Deformed cell (dashed line) subjected to sensing forces. $\mathbf{e}_{pol}$ stands for the unit vector of the polarization direction calculated via resultant traction force, $\mathbf{F}_R^{trac}$, and random protrusion force, $\mathbf{F}_{prot}$. It is of interest to note that the effect of the resultant traction force on polarization direction is more important than the one of the random protrusion force.

$\mathbf{x}_o$ is the cell centroid position vector and $\mathbf{x}_i$ is the position vector of the ith external node of the cell. Consequently, the resultant traction force, $\mathbf{F}_R^{trac}$, can be calculated as

$$\mathbf{F}_R^{trac} = \sum_{i=1}^{n} \mathbf{F}_i^{trac} \tag{1.14}$$

where n is the number of the external node of the cell.
To calculate the magnitude of the cell velocity, the vector of the protrusion force should be estimated at every step. It can be defined as

$$\mathbf{F}_{prot} = \lambda \mathbf{e}_{rand} \tag{1.15}$$

$\mathbf{e}_{rand}$ is a random unit vector. λ is the magnitude of the protrusion force which is estimated as

$$\lambda = \kappa \parallel \mathbf{F}_R^{trac} \parallel \tag{1.16}$$

where κ is a random number, $0 < \kappa < 1$. It is important to note that the magnitude of the protrusion force, λ, should be less than the traction force [26, 52].
From Eq. 1.8 and Eq. 1.10, the cell velocity can be defined as

$$v = \frac{\parallel \mathbf{F}_R^{trac} + \mathbf{F}_{prot} \parallel}{\beta \mu} \tag{1.17}$$

Thereby, at every time step, the distance through which the cell migrates to locate in its new position can be calculated. Hence, the displacement vector of the cell can be defined as

$$\mathbf{d} = v\tau \mathbf{e}_{pol} \tag{1.18}$$

where τ is time step of simulation and $\mathbf{e}_{pol}$ is a unit vector which represents direction of cell migration. It is important to note that, at every time step, the internal deformation at every cell external node, caused by the sensing force, is negative (cell exerts contraction forces toward

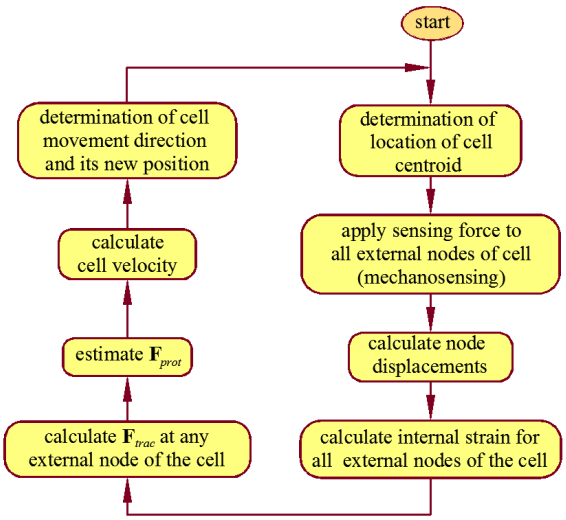

Figure 1.5: Computational algorithm of cell migration. First, the cell senses its environment. By information evaluated at that sensing step, cell can polarize and migrate after calculating traction force and estimating protrusion force.

its centroid and always tries to compress itself). Nodes with less internal deformation will have a higher traction force (note that the cell internal deformation has to be within the hatched area of Fig. 1.2-b). As all the traction forces are acting toward the cell centroid, the resultant of these traction forces will have the direction of minimum internal deformation. So that, the resultant of the traction force opposite direction and random protrusion force presents the polarization direction of the cell. Therefore, the unit vector of cell polarization, $\mathbf{e}_{pol}$, can be defined as

$$\mathbf{e}_{pol} = \frac{\mathbf{F}_{prot} - \mathbf{F}_R^{trac}}{\| \mathbf{F}_{prot} - \mathbf{F}_R^{trac} \|} \tag{1.19}$$

It is remarkable that according to the effect of the random protrusion force, $\mathbf{F}_{prot}$, the cell will move toward stiffer and/or more fixed region of the substrate (minimum deformation) in a random directed motion.

1.1.2 Cell-cell interaction

The same previous formulation is used to define traction force, protrusion force, velocity and reorientation of each individual cell. A model that defines the interaction of cells will be presented along this section. Let us define $\mathbf{r}_{ij}$ as a vector passing through centroid of two cells i and j (Fig. 1.6-a).

$$\mathbf{r}_{ij} = \mathbf{r}_j - \mathbf{r}_i \tag{1.20}$$

A useful simplification to avoid interference of two cells is that the magnitude of the $\mathbf{r}_{ij}$ should be greater than or equal to the cell diameter. In reality the cells inside a multicellular system do not preserve a spherical shape but deform to be tangent to each other and cover all the matrix [32]. In our case and for discretization, when two cells touch each other they can have a maximum of four common nodes (Fig. 1.6-b).

In vivo, the cell drives out a pseudopod to sense its environment better. Once the cell finds the stiffer region of the substrate it pulls up whole body in direction of the pseudopod [47].

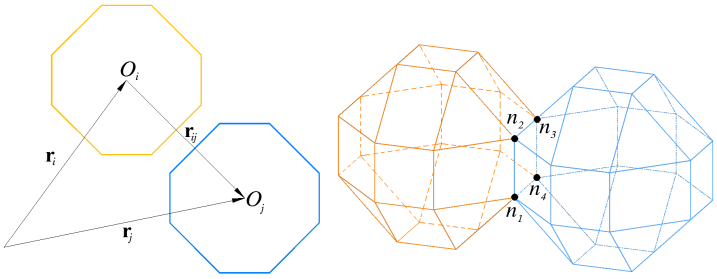

(a) (b)

Figure 1.6: (a) Distance between the centroids of two cells. (b) Interaction of two cells when they contact each other. The distance between their centroid is equal to the proposed cell diameter. Here, for assumed shape of the cell, two cells can have maximum four common nodes in this situation.

Therefore, when two or several cells touch each other, the common points of both cells (for instance nodes $n_1 : n_4$ in Fig. 1.6-b) are not able to drive out the pseudopod to substrate [8, 47]. Therefore, for two or more cells, I assume that the cells do not exert any sensing force at those nodes unless they get separated again due to the protrusion force (see Fig. 1.6-b). It is worth to note that in such situation these common nodes do not have any role to sense their environment but traction forces in those nodes are not zero.

Chapter 2

Experimental Monitoring of The Cell

Cellular microenvironments through different tissues are characterized in terms of protein composition, protein-protein interactions and the collective properties. These characteristics create variety of local elasticity and structure which make specific each tissue. The elasticity of microenvironments within brain, fat, muscle, cartilage and pre-calcified bone is ranged at Fig. 2.1 [10].
Cells within tissues constantly probe the mechanical properties of their surroundings by adhering, actively pulling, and sensing of their substrate to induced deformations. The introduction of novel techniques have not only opened up completely new perspectives regarding biological function, but also presented a new quantitative element into this field. For example, the availability of soft elastic substrates with controlled stiffness and variety of optical and florescence microscopies allows me to culture cells in different stiffness substrates to track the cell behavior. Besides numerical model approaches, these progresses enable us to work in close contact with experimental data.

To experimentally visualize cell migration in 3D substrate, I manipulated a 3D substrate with constant stiffness (Fig. 2.2). The substrate is composed of collagen I which forms a firm gel at a neutral pH and 37°C when diluted. It is a fibrous protein that is composed of three α chains which form a rope-like triple helix, providing tensile strength of ECM. The α chains contain GXY. G refers to glycine which is a small amino acid and fits well to the triple helix. X and Y are typically proline and hydroxyproline which are critical for collagen stability. Collagen type I is the most common fibrillar collagen and is mostly found in skin, bone, tendons, and other connective tissues.
After preparation of the gel, visualize of the cell in 3D collage based substrate has been performed by collaboration of Dr. Pilar Martín Duque in "Instituto Aragonés de Ciencias de la Salud (I+CS), departamento de Hospital Miguel Servet, Unidad de investigación Traslacional". I have used the florescence microscopy of this center to record the cell motility during about 24 hours.

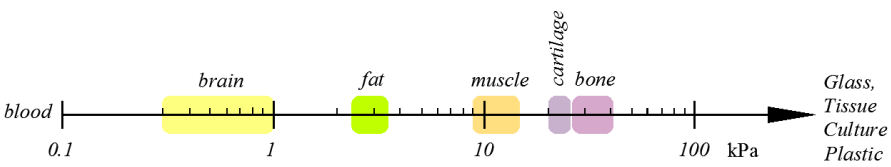

Figure 2.1: Elasticities of cellular environments [10].

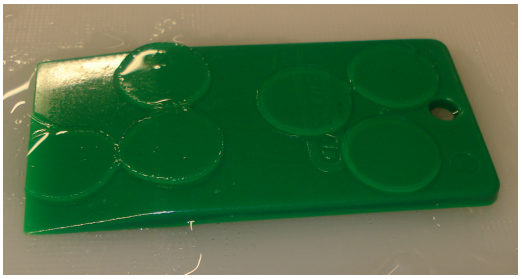

Figure 2.2: Samples of manipulated gel in the lab for cell culture.

2.1 Cell Culture

Many cell types such as fibroblasts, smooth muscle cells, epithelial cells, and endothelial cells adhere well to collagen matrices [16]. I here applied fibroblast cells to culture in 3D collagen based gel.
To prepare the cells, I seed them in a 25 cm^2 plate in 5 ml of DMEM medium. After about 24 hours when they occupy 80% of the container surface they are ready to harvest. I place the cells for 5 minutes at 37°C environment then using 2 ml trypsine/EDTA, they can be detached from container. With pipette aid, I transfer them into 5 ml of the same medium in a tube then I place it in the centrifuge at 0.3 rpm for 5 minutes.
The objective is to monitor a single cell in a 3D gel so that I seed about 1000 cells/ml which are few enough to avoid interaction between them. To count the cells I suspend the pellet in 1 ml of the same medium and then I count the cells under optic microscopy. To achieve the desired number of the cell I dilute the cells in final concentration of 1000 cells/ml. Afterwards the cells are ready to seed in the prepared gel.

2.2 Gel Manipulation

Here I describe the procedure for the preparation of 3D gel. It has been recommended to perform following procedure in a laminar flow inside biological hood and using asceptic techniques to prevent contamination [40]. To manipulate collagen based substrate, I need collagen I (5 mg/ml), sterile 10X phosphate buffered saline (PBS), sterile distilled water (dH_2O), and sterile 1N NaOH (fresh) that it is necessary to hold them on ice during preparation of gel [33]. Knowing final volume and concentration of Collagen, I need to determine the amount of each component. Here optimal concentration of gel is 4 mg/ml so that needed volume of collagen before solidification, V_1, can be determined as [33, 40]

$$V_1 = \frac{c_f V_{tot}}{c_i} \tag{2.1}$$

where V_{tot} is the desired total volume of gel, and c_i and c_f present initial and final concentration of collagen respectively. Also needed volume of 10X PBS, V_2, of 1N NaOH, V_3, and of dH_2O, V_4, can be calculated by [33, 40]

$$V_2 = \frac{V_{tot}}{10} \tag{2.2}$$

$$V_3 = 0.025 V_{tot} \tag{2.3}$$

$$V_4 = V_{tot} - (V_1 + V_2 + V_3) \tag{2.4}$$

Table 2.1: Fraction of components for a 4 mg/ml firm gel at a total volume of 10 ml collagen gel.

Component volume	V_1	V_2	V_3	V_4
amount of volume [ml]	8	1	0.2	0.8

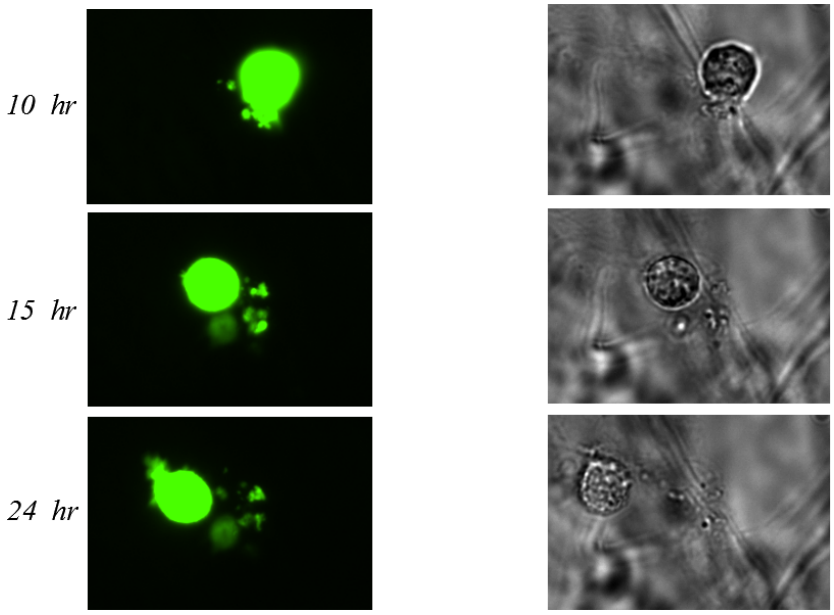

Figure 2.3: Visualization of a single cell in a 3D collagen based substrate using florescence microscopy. (a) Green florescence image, (b) bright field image.

We have cultured the cells at a total volume of 10 ml collagen gel whose the final concentration is 4 mg/ml. Required amount of gel components has been presented in table 2.1. Since amount of each component is defined I can mix dH_2O, 1N NaOH, and 10X PBS in a sterile tube. Then I slowly pipette the collagen to the tube, and I gently stir the solution to mix well. The resultant mixture must achieve a pH of 6.5-7.5 (optimal pH is 7). Because gelling may occur in room temperature, I should place the collagen into the favourable well plates or I must store the tube on ice. After seeding the cells, the medium is incubated at 37°C and 95% humidity for about 30-40 minutes or until a firm gel formation.

2.3 Cell Visualization

We successfully manipulated a 3D collagen based matrix with constant stiffness (gel concentration is 4 mg/ml). Then I used florescence microscopy to track the cell in the 3D collagen matrix. I could record the cell migration for about 24 hours. Fig. 2.3 presents two florescence and bright field images of this recorded movie during different times.

Chapter 3

Numerical Experiments

During all the next experiments, a user subroutine through the commercial software Simulia-ABAQUS FEA 6.10 was used [19]. The presented algorithm (Fig. 1.5) was run for about 100 steps with every time scale approximately equal to 10 minutes, roughly the time needed to complete one cell migration [52]. It is important to note that the time scale is variable depending on cell velocity. Of course, there exists the possibility that during several steps the velocity of the cell is too slow so that the displacement vector will not be high enough to move the cell to a new position so the cell remains in the same location. All the used parameters are summarized in Tables 3.1 and 3.2. The considered substrate dimensions are $400\times200\times200$ μm. A 3D regular mesh of hexahedrons is used with 16000 elements and 18081 nodes. I assume a sphere shape configuration for the cell (Fig. 1.3) with total number of external nodes of 24, although it may change to fit any selected configuration of the cell. The considered sensing force is about 10^{-8} N which can create a measurable deformation in the surrounding matrix in range of 30-50 μm radius, depending on the substrate stiffness [38]. A small sphere will visualize the cell centroid at every time step to indicate the cell position in Figs. 3.1 : 3.4, 3.8, 3.10, and 3.12. In the case of high cell population, for better visualization, cells will visualize as a sphere with real dimensions (Fig. 3.14).

3.1 Two different stiffness substrates with different boundary conditions

In this section, I reproduce the same experiments proposed in Borau et al. [5, 6]. The substrate is divided in two parts with different stiffness. The dimensions of both stiff and soft parts are the same ($200\times200\times200$ μm) but with three different boundary conditions (three different cases). Fig. 3.1 : 3.3 shows the obtained results in full agreement with their findings.

3.1.1 Case 1

The substrate is considered to be composed of two regions, stiff and soft. Table 3.2 illustrates the substrate properties of both parts [26, 35, 52]. As boundary condition, the surface perpendicular to the x-axis in the stiffer side is fully constrained (zero displacements) while other surfaces are free (zero tractions) (Fig. 3.1-a).
Experiments by Lo et al. [26] demonstrated that the cell tends to move toward the stiffer part.

Table 3.1: Cell parameters. *These parameters depend on cell sensing force and substrate stiffness [38].

Description	Symbol	Value	Ref.
Stiffness of microtubules	K_{pas}	2.8 kPa	[42]
Stiffness of myosin II	K_{act}	2 kPa	[42]
Maximum strain of the cell*	ϵ_1	0.09	[38]
Minimum strain of the cell*	ϵ_2	-0.09	[38]
Maximum contractile stress exerted by actin-myosin machinery	σ_{max}	0.1 kPa	[31, 35]
Surface area of the cell	S	800 μm^2	[9]
Binding constant at rear and front of the cell	$k_f = k_b$	10^8 mol^{-1}	[52]
Number of available receptors on the front	n_f	$1.5 * 10^5$	[52]
Number of available receptors on the rear	n_b	10^5	[52]
Concentration of the ligands at rear and front of the cell	ψ	10^{-5} mol	[52]

Table 3.2: Substrate properties. *This is elastic modulus of the stiff part of the substrate when the substrate is composed of two stiff and soft parts.

Description	Symbol	Value	Ref.
Substrate elastic modulus (stiff part)*	E_1	100 kPa	[52]
Substrate elastic modulus (soft part)	E_2	200 kPa	[52]
Poisson ratio	ν	0.3	[1, 50]
Viscosity	μ	1000 Pa.s	[1, 52]

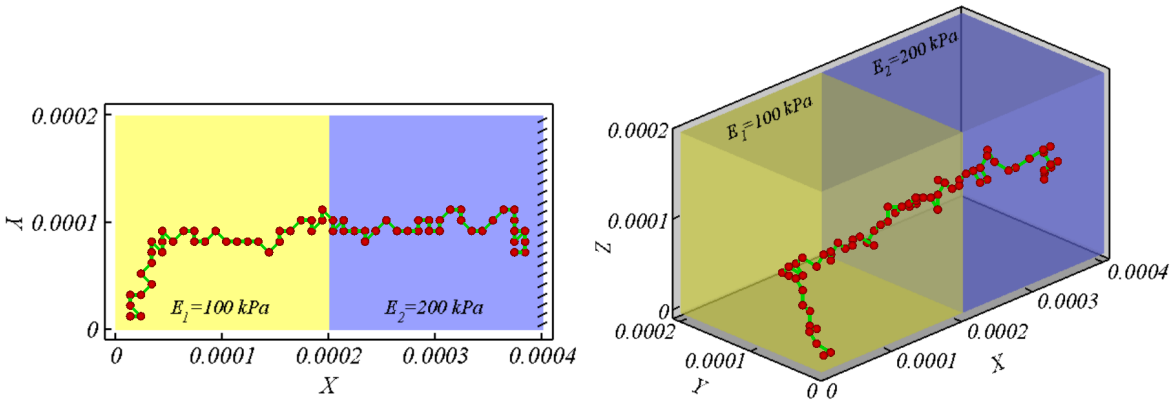

(a) (b)

Figure 3.1: Cell migration in two different stiffness substrates, case 1. The surface at the stiffer part, x=0.0004, is fully constrained. The cell is initially positioned in the softer (left) part, near to the free surfaces at the corner. The cell moves toward the stiffer (right) part and when the cell finds the constrained surface in the stiffer part, it moves randomly toward this surface and never goes far from it.

To minimize the effects of mechanical intercellular interactions through the elastic substrate, they used a low cell density and focused only on individual cells without evident neighbors in the observation field. When they seeded cells inside the soft part of the substrate, they observed that the cell moved into the stiffer side of the substrate.
Initially, the cell is located near to free surfaces in the soft part where the substrate has maximum deformation. When the cell starts to sense the substrate it recognizes the stiffer part of the substrate (right hand part in Fig. 3.1). It should be noted that the constrained surface increases the apparent stiffness near to it. Therefore, after the cell entrance into the stiffer region of the substrate it moves therefore toward the constrained surface. Once the cell catches the constrained surface, it keeps moving around it in random movement and does not deviate far from this constrained surface. (Fig. 3.1).
The cell does never go from the stiffer side to the softer one, if there was no protrusion force [26, 35]. If the effect of the random protrusion force increases, it is possible that the resultant force acting on the cell goes along the direction of the softer part. However this phenomenon does not normally occur, resulting the direction of total traction force always toward the minimum deformation region since the magnitude of the protrusion force is always lower than the traction one [26, 52]. Therefore, as a result, the cell moves consistently toward the stiffer region in a random direction movement.

3.1.2 Case 2

In this case, the substrate properties are the same as that in case 1 (Table 3.2 [26, 35, 52]) but the boundary conditions are different. Now, both surfaces perpendicular to the x-axis in the soft and stiff regions are constrained (Fig. 3.2-a). In such situation, an imaginary equilibrium plane (IEP) (the dotted line in Figs. 3.2-a and 3.2-c) appears through where the cell changes its migration behavior. Around this plane the cell receives different signals from the constrained

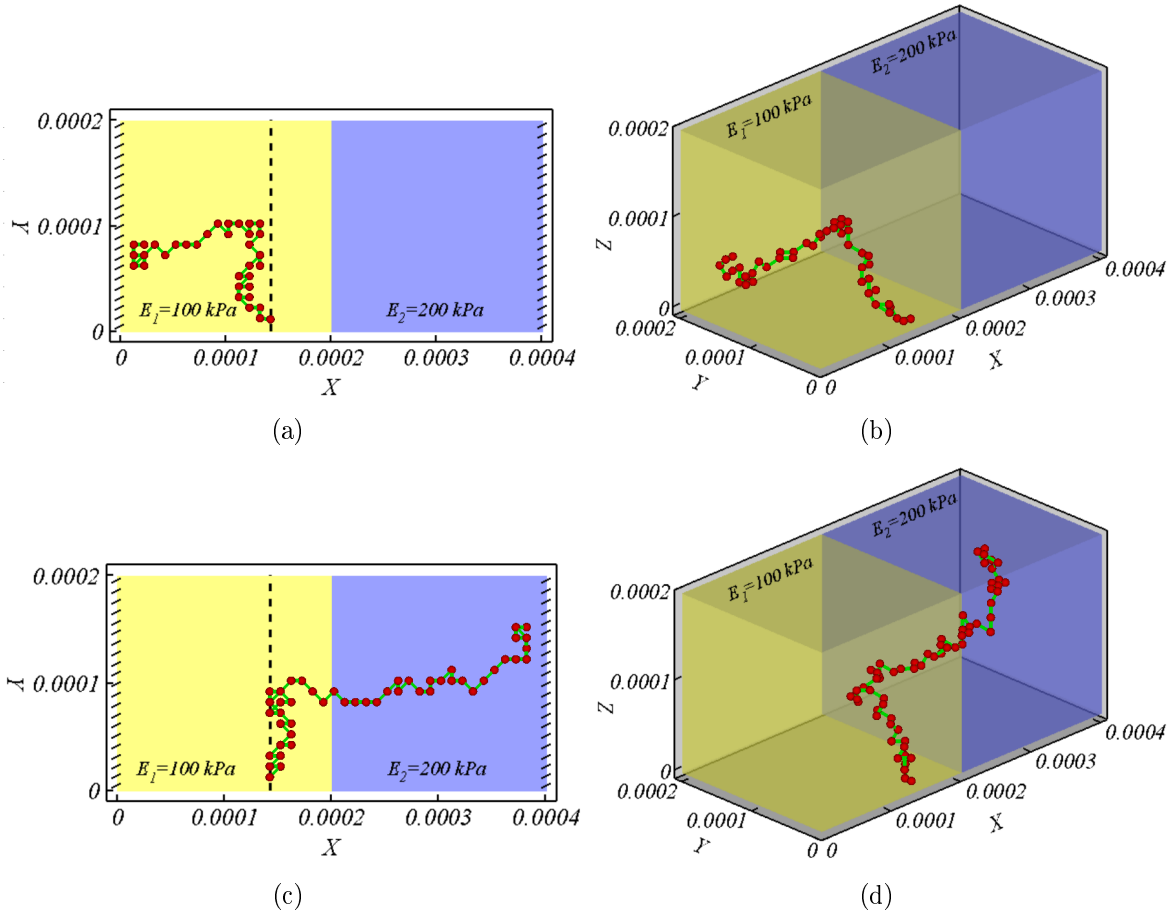

Figure 3.2: Cell migration in two different stiffness substrates, case 2. The two surfaces perpendicular to the x-axis at the both sides are constrained. In this case, an IEP appears through where the cell changes the direction of polarization. If the cell is placed in the left region of IEP, it moves toward the constrained surface in the softer part (a and b). By contrast, if the cell is initially located in the right side of the IEP the behavior of the cell changes and migrates toward the stiffer region and toward the constrained surface in the stiffer part (c and d).

surfaces or different stiffnesses regions. The location of this IEP slightly changes between different simulations due to random protrusion force.

In this case, when the cell is located close enough to the constrained surface in the softer side (left hand region of the IEP), the signal coming from that constrained wall is higher, so it moves toward this constrained boundary of the softer side (Fig. 3.2-a and 3.2-b). Alternatively, when the cell is placed in the other side of the IEP, it firstly sense the stiffness of the stiffer part of the substrate (right hand one) so it migrates toward the stiffer part and then toward the constrained surface in this side (Fig. 3.2-c and 3.2-d). In all cases, when the cell arrives to constrained surface in the stiffer or softer part it keeps moving near to this surface randomly. If the cell is initially positioned in the stiffer part it never goes to the softer part of the substrate. It is remarkable that if the cell is placed close to the IEP, its behavior depends on the relative amplitude of the protrusion force in the initial steps of its movement.

3.1.3 Case 3

Here for the same substrate I change the boundary conditions again. In this case, I restrain (zero displacements) the surface perpendicular again to the x-axis but now the one closer to the softer region leaving the rest of the boundary surfaces free (zero tractions). Two IEPs do appear (one in the softer part and another in the stiffer part) (Fig. 3.3). Therefore, there are three zones separated by these IEPs where the cell receives different feedbacks [26].

In Fig. 3.3-a and 3.3-b, when the cell is located close enough to the free surfaces in the stiffer side of the substrate, it moves away toward the interior of the substrate. Once the cell finds the first IEP, in the stiffer region, it keeps moving near to it randomly. If the cell is initially positioned between the two IEPs (Fig. 3.3-c and 3.3-d), no matter if in the stiffer or softer parts of the substrate, it again moves toward the IEP in the stiffer part.
By contrast, if the cell is placed in the left hand side of the IEP placed in soft part (left hand IEP) the polarization of the cell changes and the cell moves toward the constrained surface in the softer side as seen in Fig. 3.3-e and 3.3-f.

3.2 Effect of a stiffness gradient

To fully understand the effect of the stiffness on cell migration I applied the proposed model to a substrate with linear stiffness gradient which changes from 100 kPa at $x = 0$ to 200 kPa at $x = 400$ μm through which all the substrate surfaces are considered free.
Hadjipanayi et al. [17] analyzed the effect of a 3D substrate with linear stiffness gradient on cell migration. They divided this substrate into soft, middle, and stiff regions. First, they inserted about the same number of cells inside these zones. Since the number of cells was few, they assumed that there was no interaction among cells. After 6 days, they observed a significant difference in cell concentration in these three regions. They observed that the higher cell concentration resulted in the stiffer part while the least concentration was identified in the softer.
In our simulation, and as expected when a cell is placed in this substrate, the cell tendency is to migrate toward the direction of the higher stiffness (Fig. 3.4). When all boundary surfaces are considered free, the cell randomly moves around an IEP far enough from those free surfaces located in the stiffer side. In this case, the results neither depend on the initial location of the cell (Fig. 3.4) nor the stiffness gradient. Here, only the results of the simulation corresponding to two initial different locations of the cell are presented (Fig. 3.4). This simulation was repeated for several values of the stiffness gradient and initial position of the cell and all results were consistent and in agreement with the experimental results [17].
While the cell migrates from a soft part to stiffer one, the nodal traction forces at external nodes increase. This happens because in stiffer regions, cell internal strain decreases while cell stress increases (hatched area in Fig. 1.2-b). In Fig. 3.5, the nodal traction force corresponding to one of the external nodes of the cell has been plotted. On the contrary, the net traction force affecting on cell migration decreases (Fig. 3.6). This happens because while the nodal traction forces increase, differences between them decrease and consequently the net traction force reduces. This explains why the cell in stiffer parts generally remains round and symmetric whereas it exerts higher nodal traction forces. This result is corroborated by findings of Ehrbar et al. [13]. It is worth to remark that curve fluctuation in Figs. 3.5 and 3.6 is due to the effect

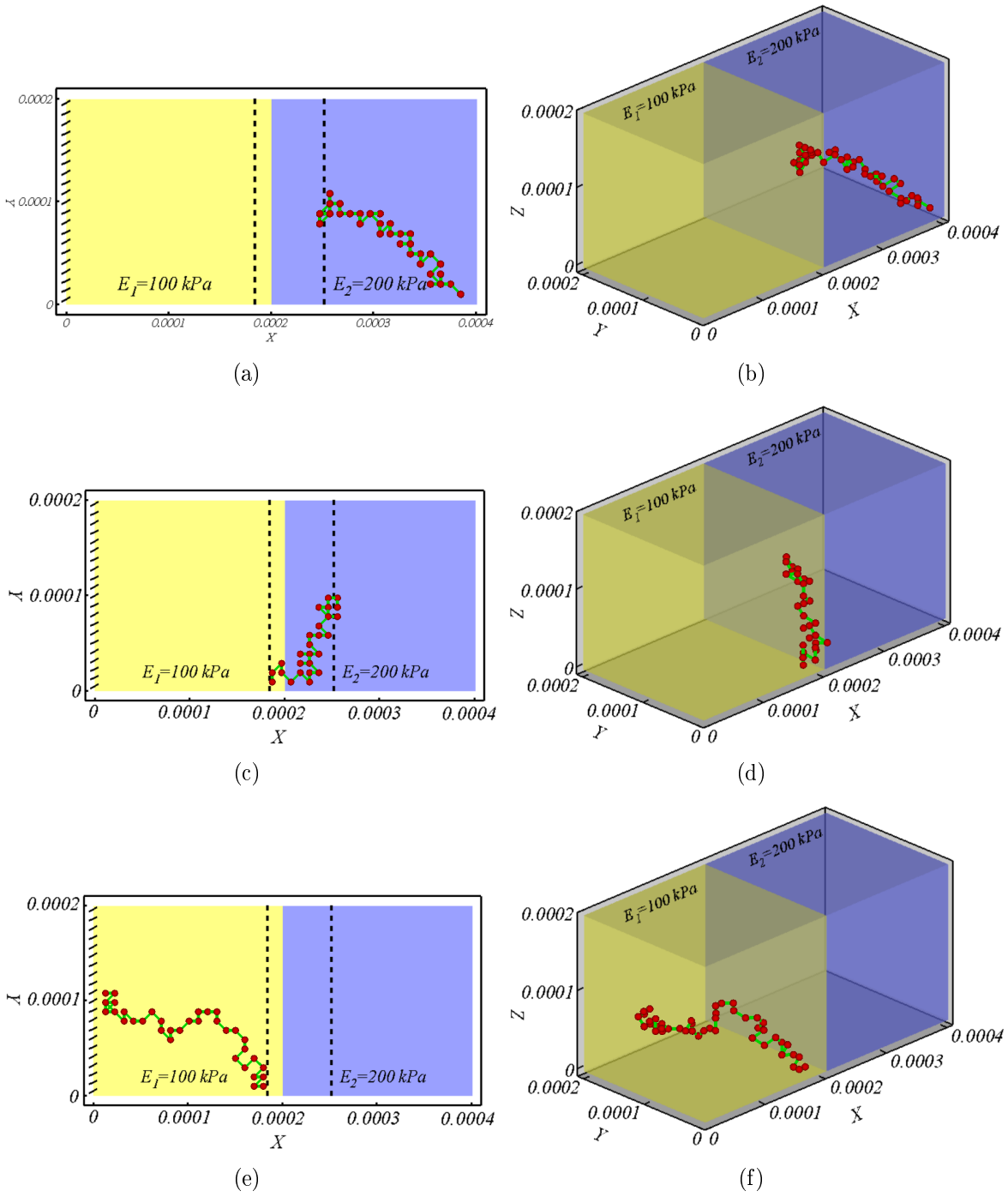

Figure 3.3: Cell migration in two different stiffness substrates, case 3. The surface in the softer part has been restrained leaving the rest free. In this case, two IEPs appear, one in the stiffer part and another in the softer part. If the cell is initially placed in the right side of the IEP located in the stiffer part (a and b) or between these IEPs (c and d), it migrates toward the IEP placed inside the stiffer region. If the cell is firstly seeded in the left side of the IEP located in the softer part it migrates toward the constrained surface in the softer region (e and f).

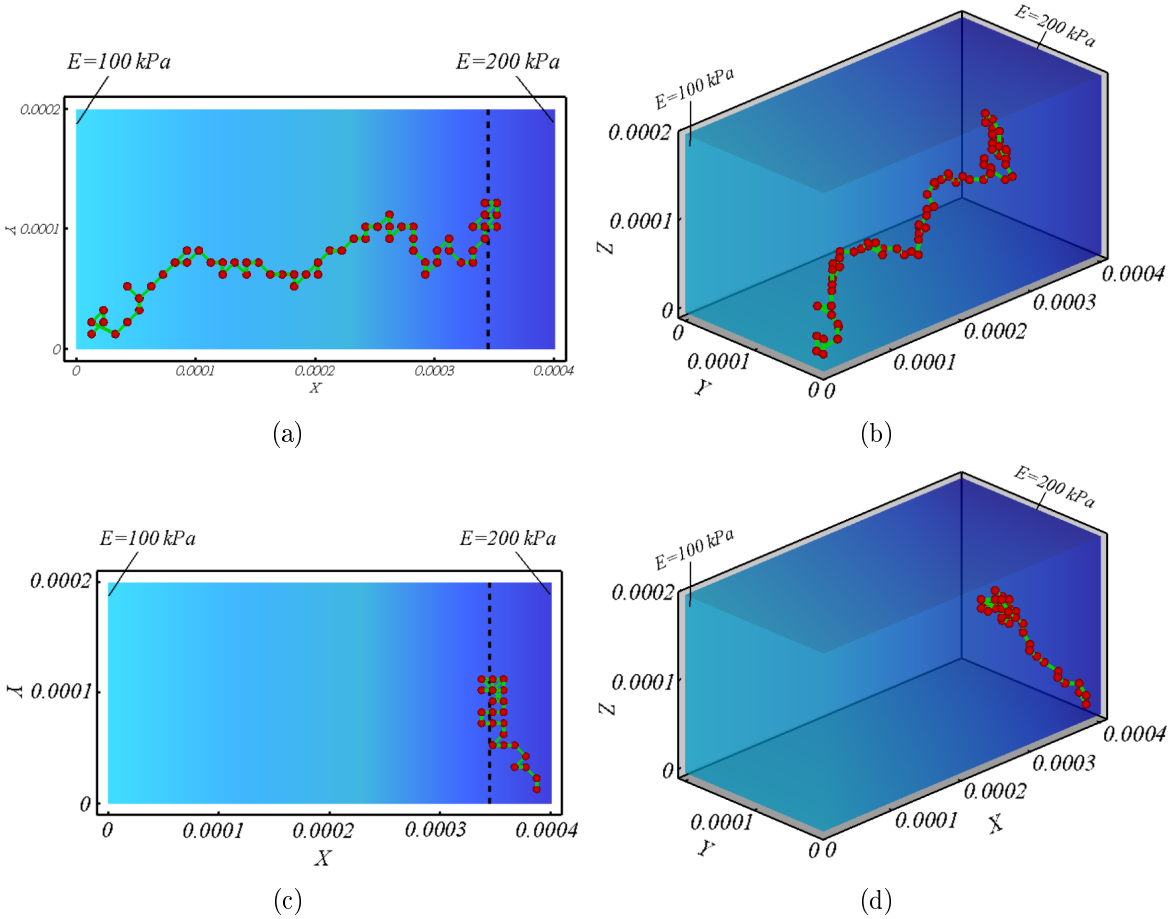

Figure 3.4: Cell migration in a substrate with a stiffness gradient and free boundary surfaces. In the first case (a) and (b), cell has been embedded in one of the corners of the substrate (softer side), it migrates toward the IEP (dotted line) far enough from free surfaces and keeps moving randomly around it. In the second case (c) and (d), the cell starts to migrates from the stiffer side toward the softer one until the IEP and keeps moving around it.

of the cell protrusion force.
Fig. 3.7 shows how the overall cell velocity decreases during cell migration toward stiffer regions. This means that the low net traction force in stiffer zones causes low cell speed which can even stop cell migration in very dense substrates [13, 52]. On the other hand, the oscillations of the cell velocity in Fig. 3.7 seem to have higher amplitude than that of nodal traction forces and net traction force in Figs. 3.5 and 3.6. This is because the protrusion force affects not only on the direction of cell migration but also on the magnitude of the cell velocity. It is clear that when the cell approaches the IEP, after about 80 time steps, the studded parameters tend to be more stable since the local strains of the cell do not change too much.

3.3 Effect of substrate depth

The proposed model was applied for a substrate with a slope as seen Fig. 3.8 to study the effect of substrate depth on cell migration. Here the sloped surface has been constrained and

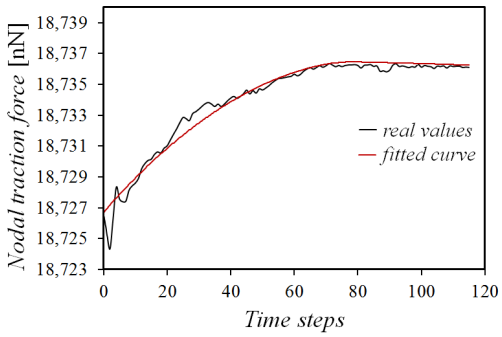

Figure 3.5: The effect of the substrate stiffness on the cell nodal traction force during migration.

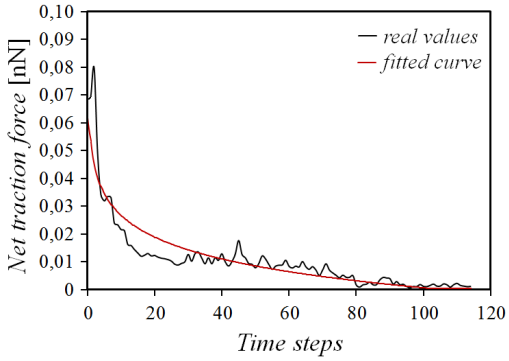

Figure 3.6: The effect of the substrate stiffness on the cell net traction force during migration.

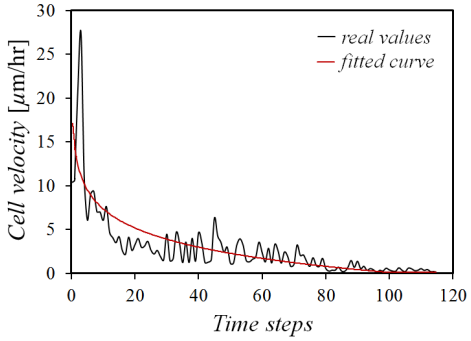

Figure 3.7: The effect of the substrate stiffness on the cell migration velocity.

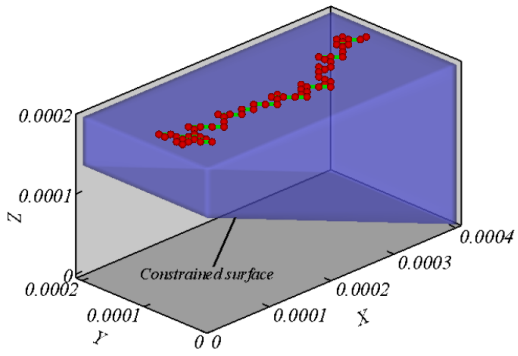

Figure 3.8: Migration of the cell due to the variance of substrate depth. The sloped surface is constrained.

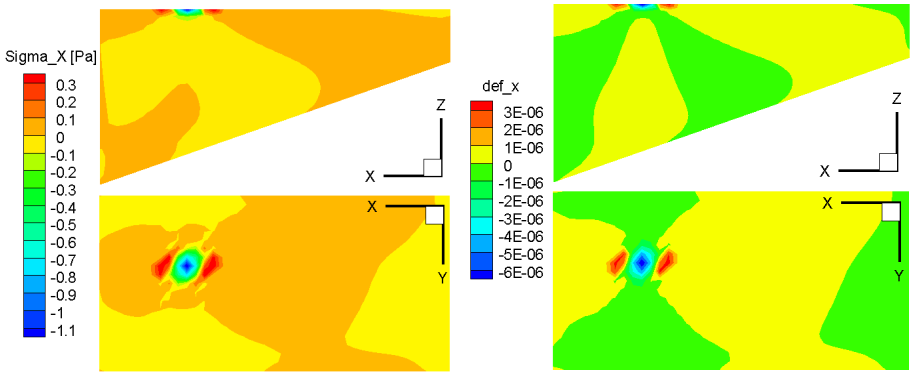

(a) (b)

Figure 3.9: Stress and deformation in x direction during sensing process.

the rest of surfaces are free. Elastic modulus of the substrate is assumed to be 100 kPa. In this experiment the cell moves over the substrate surface. Because the sloped surface is constrained, the cell will sense less internal deformation for lower depth. The cell started the migration process in a point on the substrate surface that has maximum depth. When the cell exerts sensing forces, it recognizes the direction of the slope, therefore it migrates toward minimum depth in a random path. Fig. 3.9 demonstrates an intense difference of sensing domain between the substrate surface and substrate depth. Here, since the cell exerts sensing force at the substrate surface, the z component of the sensing force is close to zero, so that the cell can not sense too deep. Consequently, due to this limitation, the speed of propagation of the cell on the surface is less than that of the cell inside three dimensional domains. This explains why the cell moves more randomly in surface migration [26].

3.4 Interaction between two cells

As cited in previous sections, the developed model can simulate cell migration with any number of cells in the populations. Hence, to fully understand the interaction between two cells, a substrate with the same dimensions of the one with stiffness gradient is employed to simulate the behavior of two cells in the same substrate (Fig. 3.10). All boundary surfaces of the substrate are considered free. The substrate elastic modulus is constant and equal to 100 kPa.

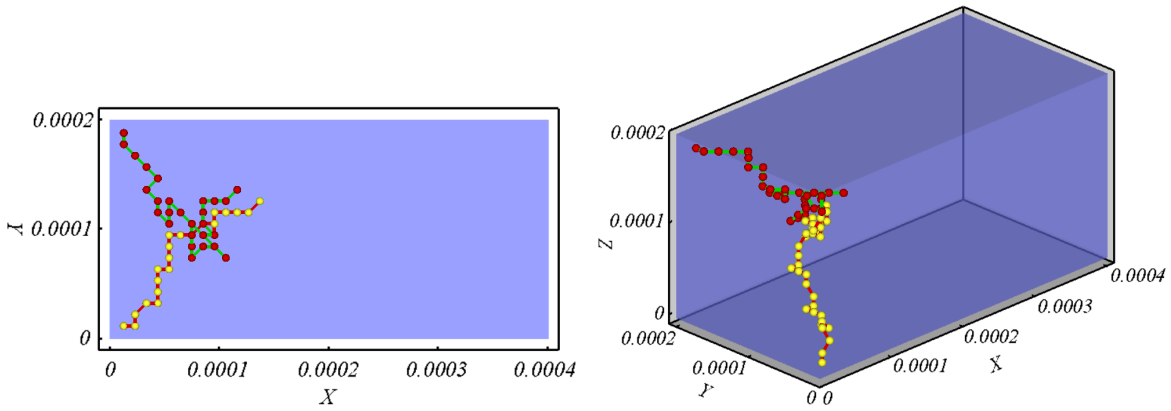

(a) (b)

Figure 3.10: Interaction between two cells inside a substrate with constant elastic modulus. All boundary surfaces of the substrate are considered free. Cells start to move from two corners of the substrate. They migrate toward the center of the substrate and keep move around each other randomly.

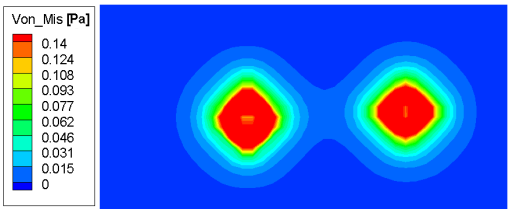

Figure 3.11: Von Mises stresses due to mechanosensing of two cells during migration. The stretched zone between two cells is clear because of their interaction.

Near to the free surfaces, one cell is located in the top corner of the substrate and another in the bottom corner of the substrate. It should be again mentioned that a red and yellow sphere represent the centroid of the each cell. As we observe in Fig. 3.10, both cells migrate in a random path toward each other. Once they sense each other in the middle of the substrate, they keep moving around each other randomly. As mentioned earlier, the cell exerts contraction sensing forces at its external nodes toward its centroid to feel its environment. So, when cells are sufficient near to each other, the region between them will be under tension (Fig. 3.11). Consequently, cells will feel less internal deformation in this direction. They will detect this zone as stiffer region of the substrate and migrate toward each other. Once they contact each other as long as their polarization direction is either toward each other or in the same direction they remain in contact. When, their polarization directions become different they separate until they regain contact and so on.

To better understand the effect of this phenomenon of cell migration, simulations were repeated for the previous substrate with stiffness gradient. The results are in agreement with migration of one cell inside the substrate with constant stiffness as seen in Fig. 3.12. Firstly, the cells try to reach each other and after crossing the first quarter of the x-axis, they continue to move together toward the stiffer region of their substrate. Again, and as in case of individual cell, there exists an IEP where cells maintain moving together randomly around it. Fig. 3.13 shows the curve of cell velocity for one and two cells migration. To compare the cell velocities in both

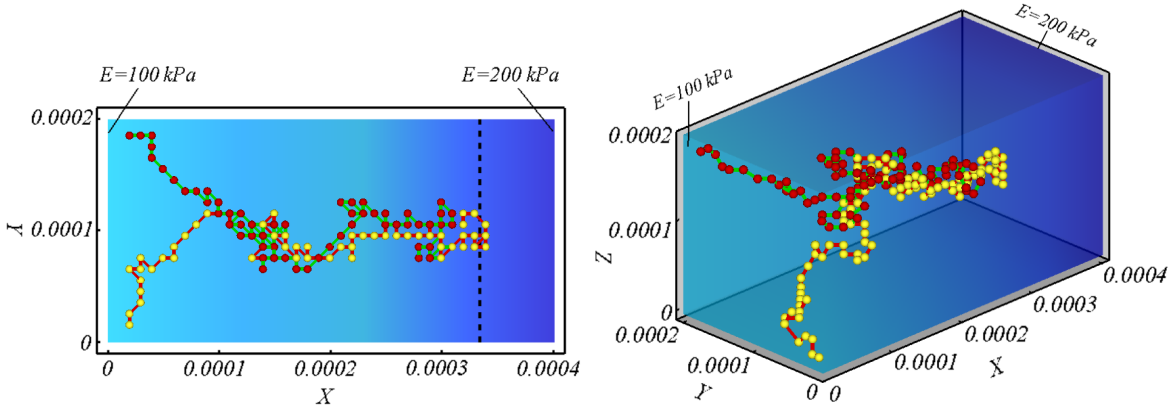

(a) (b)

Figure 3.12: Interaction between two cells inside a substrate with stiffness gradient. All the boundary surfaces of the substrate are considered free. Two cells start to move from two corners of the substrate.

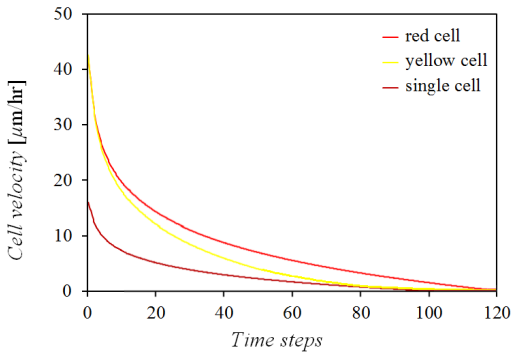

Figure 3.13: Comparison of cell migration velocities for two cells and single cell migration.

cases, I fitted an average curve for each cell velocity to eliminate the velocity fluctuation due to the protrusion force. The simulations were repeated several times and the result was similar. The figure shows that the overall cell velocity in case of single cell migration is less than two-cell migration. This is because in the case of two cells, the nodes near to the stretched area between the two cells experience less deformation (Fig. 3.11). On the contrary, the nodes that are away from this area in the other side of the cell will experience more deformation and less traction force. The local cell velocity for two-cell migration is higher than the one for single cell. In this case, the number of steps needed by the cell to catch the IEP was about 130 time steps which is higher than in case of one cell.

3.5 Cell population

In this experiment, the proposed model is employed to simulate a cell population with 40 cells simultaneously embedded inside a substrate with the same dimensions as that of the previous experiment. All boundary surfaces of the substrate are considered free. Elastic modulus is considered to be constant throughout the substrate (100 kPa). At the beginning, the cells are randomly distributed near the boundary surfaces (Fig. 3.14-a). When cells exert the sensing

force to check their environment, they recognize the middle of the substrate as a more stable region. Fig. 3.14 represents cells locomotion for different time steps. Here, for better representation of cell-cell interaction and their contacts, I represented the proposed sphere shape configuration of the cells in each step. During migration, several stretched zones exist between cells that affect cell locomotion. So that, in primary steps of migration, they aggregate in small groups (Fig. 3.14-b). Joining these slugs to each other, several big slugs of the cells are formed (Fig. 3.14-c). Afterward, all this slugs contact each other in the middle of the substrate (Fig. 3.14-d). Internal cells which are enveloped by several cells stop moving, but boundary cells may move around enveloped cells. Upon a cell inside the slug reach circumference of the cell aggregation, it will have possibility to move around the cell aggregation. In this simulation the cells respond similarly and consistently as previous experimental [30] and numerical works [32].

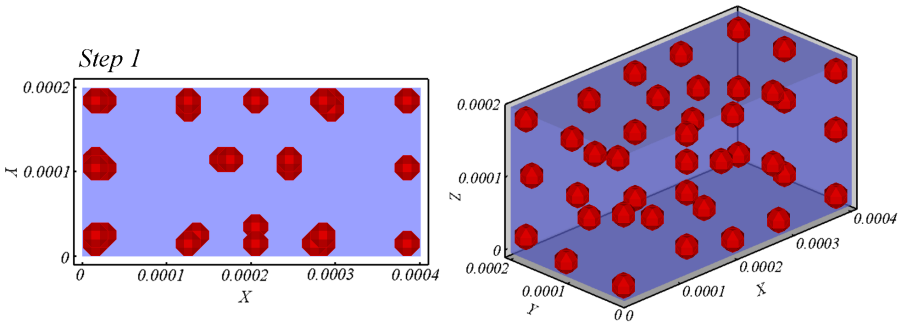

(a)

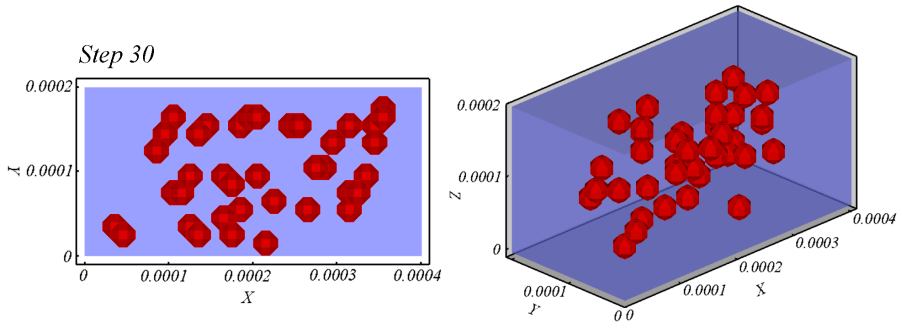

(b)

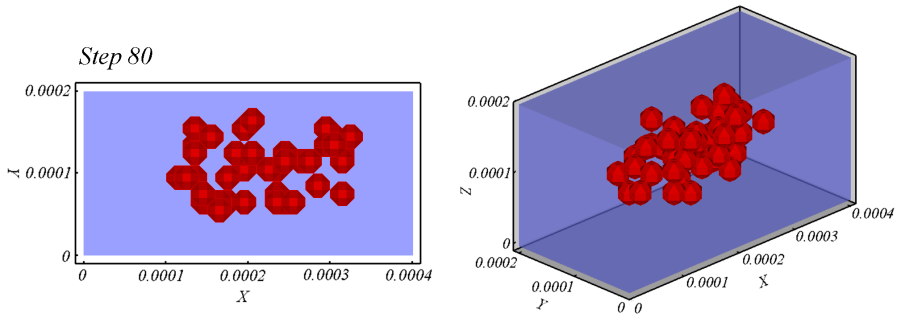

(c)

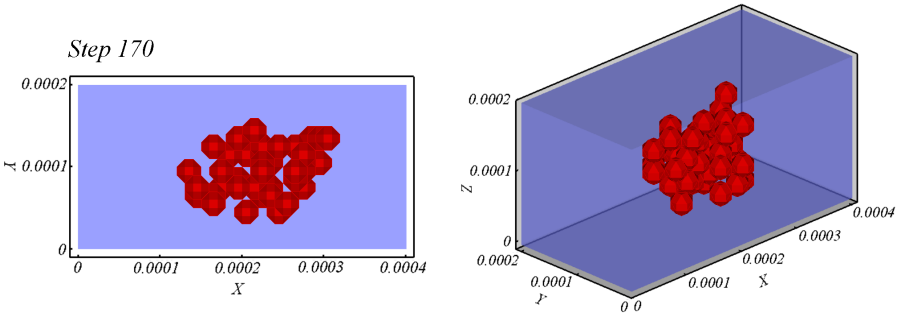

(d)

Figure 3.14: Interaction between 40 cells inside a substrate with free boundary surfaces. During the locomotion, cells tend to contact forming small slugs and then they attach each other in center of the substrate to create an aggregation of cells.

Conclusions and Future Works

Conclusion

I have developed a three-dimensional computational model to simulate cell migration with the initial aim of analyzing how substrate stiffness and its boundary conditions guide cell migration and how the cells interact each other inside the same substrate. I qualitatively validated the obtained results with experimental observations [10, 17, 26, 30, 35] and with previous numerical models [5, 6, 9, 32].

I applied our model for several experiments to understand the role of the boundary conditions, stiffness gradient, substrate depth and cell-cell interaction in cell migration. As observed in the results shown above, any change in the boundary conditions may change the the cell final position and locomotion path. When there are constrained surfaces, the primary position of the cell becomes important. In general, the cell migrates toward stiffer or more fixed parts in its neighbors. But, as observed in the presented experiments, in some cases, the cell cannot move toward the stiffer region of the substrate. For example, when the initial location of the cell is close to a constrained wall in the softer part, the signal from this wall may be higher than that coming from the stiffer region. In such situations and depending on the boundary conditions, it may appear one (Figs. 3.2) or two (Figs. 3.3) IEPs which separate different parts in which the cell displays different behaviors.

For a substrate with stiffness gradient, there exists an IEP toward which the cell always tends to migrate. Once the cell catches it, it keeps moving around it far from free boundary surfaces. In this case, the primary position of the cell is not important. Again and as exception, the cell tends to migrate from stiffer to softer regions (Figs. 8-c and 8-d). The obtained results demonstrate that during cell migration from a softer toward a stiffer region, nodal traction forces increase while net traction force as well as cell velocity decrease. Reduction of net traction force causes the cell to be more rounded and symmetric [13]. This finding describes why the cell stability enhances in stiffer regions. In very stiff substrates, generated net traction forces may not be enough to move the cell to a new position.

Applying the proposed model for an individual cell migrating over the matrix surface, the results demonstrate that the cell tendency is to migrate toward minimum depth (Figs. 3.8). However, its sensing radius on surface movement is higher in comparison with its depth feeling (Figs. 3.9), notably depending on several factors as cell type, sensing forces, depth of substrate and matrix stiffness. Our finding in this case is also qualitatively consistent with previous experimental [9] and numerical results [10].

The obtained results demonstrate that interaction between two cells inside a substrate causes decay in their mean velocity toward stiffer regions due to the tendency of cells to maintain contact. This phenomenon occurs due to presence of a stretched region between the two cells created by contraction forces exerted by cells. As expected, this process also happens for cell

populations with a higher number of cells. When there are several cells inside a substrate, if the zone between one cell and other in its neighborhood is stretched enough such that the signal coming from this stretched region becomes higher than that coming from any other mechanical conditions, cells tend to be gathered forming small slugs. In the case of free boundary substrate, these created slugs will then attach to each other and aggregate in the middle of substrate (Fig. 3.14). This process can be seen in sorting of different cells [32] or in modulation of epithelial tissue [12].
As the magnitude of the cell velocity, nodal traction forces and net traction force depend on the cell type and the elastic modulus of matrix, the presented model can be a helpful tool to predict all these parameters. Besides, it is capable to predict the cell behavior for any kind of cell shape and substrate. So, I think that the proposed model can be used to simulate in vivo or in vitro experiments to anticipate the behavior of single or high population of cells. In fact, more sophisticated experiments not only can verify or refute predictions of numerical models such as the one here described, but also can determine other effective factors that may act on cell migration in vivo. However, additional experimental works are needed to fully understand the exact role of the mechanical conditions on cell behavior and cell-cell interaction.

Future works

As mentioned above, this work purely investigates effect of mechanical factors on cell migration, such as substrate stiffness, boundary conditions, substrate depth and cell-cell interaction. I will also extend this numerical model to consider chemical and topographical effects on cell migration. Moreover, through this numerical model I ignored external forces acting on cell-substrate system that I can improve model to take into account effect of this external forces.

Publications

As a result of this thesis several articles have been published in journals and proceedings of international conferences.

Journal publicarion

1. S.J. Mousavi, M.H. Doweidar and M. Doblaré (2012): Computational modelling and analysis of mechanical conditions on cell locomotion and cell-cell interaction, Computer Methods in Biomechanics and Biomedical Engineering, DOI:10.1080/10255842.2012.710841.

Conference papers

1. M.H. Doweidar, S.J. Mousavi, and M. Doblaré. Computational modelling of cell migration. 18th European Society of Biomechanics(ESB), Lisbon, Technical University of Lisbon, July 2012.
2. M.H. Doweidar, S.J. Mousavi, and M. Doblaré. Effect of ECM Stiffness Gradient on Cell Migration: A 3D Finite Element Method. 17th European Society of Biomechanics(ESB), Queen Mary, university of London, September 2011.

Bibliography

[1] S.K. Akiyama and K.M. Yamada. The interaction of plasma fibronectin with fibroblastic cells in suspension. *Journal of Biological Chemistry*, 260:4492–4500, 1985.

[2] R. Allena and D. Aubry. ?run-and-tumble? or ?look-and-run?? a mechanical model to explore the behavior of a migrating amoeboid cell. *Journal of Theoretical Biology*, 306:15–31, 2011.

[3] H. Behesti and S. Marino. Cerebellar granule cells: Insights into proliferation, differentiation, and role in medulloblastoma pathogenesis. *Journal Applied Physiology*, 41:435–445, 2009.

[4] A.D. Bershadsky, N.Q. Balaban, and B. Geiger. Adhesion-dependent cell mechanosensitivity. *Annu Rev Cell Dev Bio*, 19:677–695, 2003.

[5] C. Borau, M.H. Doweidar, and J.M. Garcia-Aznar. Modeling of cell migration and mechano-sensing in 3d. 17th Congress of the European Society of Biomechanics. Edinburgh, UK, 5-8 July 2010.

[6] C. Borau, R.D. Kamm, and J.M. García-Aznar. Mechano-sensing and cell migration: a 3d model approach. *Journal Physical Biology*, 8:1078–88, 2011.

[7] G.W. Brofland, D. Viens, and J.H. Veldhuis. A new cell-based fe model for the mechanics of embryonic epithelia. *Computer Methods Biomech. Biomed. Engin.*, 10:121–128, 2007.

[8] G.W. Brofland and C.J. Wiebe. Mechanical effects of cell anisotropy on epithelia. *Computer Methods Biomech. Biomed. Engin.*, 7:91–99, 2004.

[9] A. Buxboim, I.L. Ivanovska, and D.E. Discher. Matrix elasticity, cytoskeletal forces and physics of the nucleus: how deeply do cells 'feel' outside and in? *Journal of cell science*, 123:297–308, 2010.

[10] A. Buxboim, K. Rajagopal, A.E.X. Brown, and D.E. Discher. How deeply cells feel: methods for thin gells. *Journal Physics Condens Matter*, 22, 2010.

[11] M. Chiquet, L. Gelman, R. Lutz, and S. Maier. Wound healing: aiming for perfect skin regeneration. *Biochimica et Biophysica Acta journal*, 1973:911–920, 2009.

[12] B.A. Dalton, X.F. Walboomers, M. Dziegielewski, M.D.M. Evans, S. Taylor, J.A. Jansen, and J.G. Steele. Modulation of epithelial tissue and cell migration by microgrooves. *Phil. Trans. Roy. Soc. London*, 56:195–207, 2001.

[13] M. Ehrbar, A. sala, P. Lienemann, A. Ranga, K. Mosiewicz, A. Bittermann, S. C. Rizzi, and F. E. Weber. Elucidating the role of matrix stiffness in 3d ceell migration and remodeling. *Biophysical Journal*, 100:284–293, 2011.

[14] H.P. Ehrlich and J.B. Rajaratnam. Cell locomotion forces versus cell contraction forces for collagen lattice contraction: an in vitro model of wound contraction. *Tissue Cell*, 22:407–417, 1990.

[15] F. Graner and J. Glazier. Simulations of biological cell sortin using a two-dimensional extended potts model. *Phys. Rev. Lett.*, 69:2013–2016, 1992.

[16] F. Grinnell and W.M. Petroll. Cell motility and mechanics in three-dimensional collagen matrices. *Cell Dev. Biol.*, 26:335–61, 2010.

[17] E. Hadjipanayi, V. Mudera, and R.A. Brown. Guiding cell migration in 3d: A collagen matrix with graded directional stiffness. *Cell Motility and the Cytoskeleton*, 66:435–445, 2009.

[18] A.K. Harris, P. Wild, and D. Stopak. Silicone rubber substrata: a new wrinkle in the study of cell locomotion. *science*, 208:177–179, 1980.

[19] Hibbit, Karlson, and Sorensen. *Abaqus-Theory manual*, 6.3 edition edition.

[20] D.E. Ingber and I. Tensegrity. Cell structure and hierarchical systems biology. *Journal Cell Science*, 116:1157–1173, 2003.

[21] D.W. James and J.F. Taylor. The stress developed by sheets of chick fibroblasts in vitro. *Experimental Cell Research*, 54:107–110, 1969.

[22] R.L. Juliano and S. Haskill. Signal transduction from the extracellular matrix. *journal cell biology*, 120:577–585, 1993.

[23] D.A. Lauffenburger and A.F. Horwitz. Cell migration: a physically integrated molecular process. *Cell*, 84:359–369, 1996.

[24] J. Lee, A. Ishihara, G. Oxford, B. Johnson, and K. Jacobson. Regulation of cell movement is mediated by stretch-activated calcium channels. *Nature*, 400:382–386, 1999.

[25] K.R. Levental, H. Yu, L. Kass, J.N. Lakins, M. Egeblad, J.T. Erler, S.F.T. Fong, K. Csiszar, Am. Giaccia, W. Weninger, M. Yamauchi, D.L. Gasser, and V.M. Weaver. Matrix cross linking forces tumor progression by enhancing integrin signaling. *Cell*, 139:891–906, 2009.

[26] C.M. Lo, H.B. Wang, M. Dembo, and Y.L. Wang. Cell movement is guided by the rigidity of the substrate. *Biophysical Journal*, 79:144–152, 2000.

[27] P. Martin. Wound healing: aiming for perfect skin regeneration. *Science*, 276:75– 81, 1997.

[28] P. Moreo, J.M. Garcia-Aznar, and M. Doblaré. Modeling mechanosensing and its effect on the migration and proliferation of adherent cells. *Acta Biomaterialia*, 4:613–621, 2008.

[29] R. Nossal. On the elasticity of cytoskeletal networks. *Biophys. Journal*, 53:349–359, 1988.

[30] G.M. Odell and J.T. Bonner. How the dictyostelium discoideum grex crawls. *Phil. Trans. Roy. Soc. London*, 312:487–525, 1986.

[31] G.F. Oster, J.D. Murray, and A.K. Harris. Mechanical aspects of mesenchymal morphogenesis. *journal Embryol Exp Morph*, 78:83–125, 1983.

[32] E. Palsson. A three-dimensional model of cell movement in multicellular systems. *Future Generation Computer System*, 17:835–852, 2001.

[33] D. Park, D. Choi, H. Ryu, H. Kwon, H. Joo, and C. Min. A well-defined in vitro three-dimensional culture of human endometrium and its applicability to endometrial cancer invasion. *Cancer Letters*, 195:185–192, 2003.

[34] R.J. Pelham, Jr., and Y.L. Wang. Cell locomotion and focal adhesions are regulated by substrate flexibility. *PNAS*, 94:13661–13665, 1997.

[35] C.G. Penelope and P.A. Janmey. Cell type-specific response to growth on soft materials. *Journal Applied Physiology*, 98:1547–1553, 2005.

[36] T. Pompe, S. Glorius, T. Bischoff, I. Uhlmann, M. Kaufmann, S. Brenner, and C. Werner. Dissecting the impact of matrix anchorage and elasticity in cell adhesion. *Biophysical Journal*, 97:2154–2163, 2009.

[37] I. Ramis-Conde, D. Drasdo, A.R.A. Anderson, and M.A.J. Chaplain. Modelingthe influence of the e-cadherin–b-catenin pathway in cancer cell invasion: a multiscale approach. *Biophysical Journal*, 95:155–165, 2008.

[38] S. Ramtani. Mechanical modelling of cell/ecm and cell/cell interactions during the contraction of a fibroblast-populated collagen microsphere:theory and model simulation. *Journal of Biomechanics*, 37:1709–1718, 2004.

[39] D.E. Rassier, B.R. MacIntosh, and W. Herzog. Length dependence of active force production in skeletal muscle. *Journal Applied Physiology*, 86:1445–1157, 1999.

[40] T.M. Ritty and J. Herzog. Tendon cells produce gelatinases in response to type i collagen attachment. *Cancer Letters*, 21:442–50, 2003.

[41] N. Savill and P. Hogeweg. Modeling morphogenesis: from single cells to crawling slugs. *Journal of Theoret. Biol.*, 184:229?235, 1997.

[42] A. Schäfer and M. Radmacher. Influence of myosin ii activity on stiffness of fibroblast cells. *Acta Biomaterialia*, 1:273–280, 2005.

[43] M.P. Sheetz, D. Felsenfeld, C.G. Galbraith, and D. Choquet. Cell migration as a five-step cycle. *Biochem. Soc. Symp*, 65:233–243, 1997.

[44] Y.T. Shiu, S. Li, W.A. Marganski, S. Uami, M.A. schwartz, Y.L. Wang, M. Dembo, and S. chien. Rho mediates the shear-enhancement of endothelial cell migration and traction force generation. *Biophysical Journal*, 86:2558–2565, 2004.

[45] J.A. Spudich. The myosin swinging cross-bridge model. *Nat Rev Mol Cell Biol*, 2:387–392, 2001.

[46] S. Suresh. Biomechanics and biophysics of cancer cells. *Acta Biomaterialia*, 3:413–438, 2007.

[47] D.L. Taylor, J. Heiple, Y.L. Wang, E.J. Luna, L. Tanasugarn, J. Brier, J. Swanson, M. Fechheimer, P. Amato, M. Rockwel, and G. Daley. Cellular and molecular aspects of amoeboid movement. *CSH Symp. Quant. Biol.*, 46:101–111, 1982.

[48] S. Timoshenko and J.N. Goodier. *Theory of elasticity*. New York: Mc Graw-Hill Publishing Co, 1970.

[49] R.T. Tranquillo, D.A. Lauffenburger, and S.H. Zigmond. A stochastic model for leukocyte random motility and chemotaxis based on receptor binding fluctuations. *JCB*, 106:303–309, 1988.

[50] T.A. Ulrich, E.M. De Juan Pardo, and S. Kumar. The mechanical rigidity of the extracellular matrix regulates the structure, motility, and proliferation of glioma cells. *Cancer Research*, 69:4167–4174, 2009.

[51] H.C. Wong and W.C. Tang. Finite element analysis of the effects of focal adhesion mechanical properties and substrate stiffness on cell migration. *journal of Biomechanics*, 44:1046–50, 2011.

[52] M.H. Zaman, R.D. Kamm, P. Matsudaira, and D.A. Lauffenburgery. Computational model for cell migration in three-dimensional matrices. *Biophysical Journal*, 89:1389–1397, 2005.